J Chim Phys (1995) 92, 248-263

Time-resolved and product angle-velocity measurements of $(CH_3I)_n$ cluster photodissociation

JA Syage

The Aerospace Corporation, PO Box 92957/M5-754, Los Angeles, CA 90009, USA

We present a study of the photodissociation of CH_3I to CH_3 + I in an isolated molecule and in clusters. In previous picosecond pump-probe studies of photodissociation in clusters, we observed very fast sequential radical chemistry. An important recurring reaction is $CH_3 + CH_3I \rightarrow C_2H_6 + I$. In this paper we present new measurements of the I atom anisotropy and kinetic energy distribution from cluster photodissociation and make comparisons to similar measurements in bare CH_3I. Using a new photofragment imaging technique for measuring angle-velocity distributions, we measured an I atom kinetic energy distribution for cluster photodissociation that is substantially broader and of lower energy than that observed for monomer photodissociation. The angular distribution is essentially isotropic in the former case as opposed to highly anisotropic in the latter case.

Cet article présente l'étude de la photodissociation de CH_3I en CH_3 + I dans la molécule isolée et dans les agrégats. Nos expériences antérieures de photodissociation dans les agrégats utilisant la technique pompe -sonde picoseconde ont mis en évidence des réactions très rapides et séquentielles à partir d'espèces radicalaires. L'intérêt de cette étude se justifie par l'importance de la réaction $CH_3 + CH_3I \rightarrow C_2H_6 + I$. Nous présentons de nouvelles mesures de l'anisotropie de l'iode atomique formé à partir de la photodissociation de l'agrégat et de sa distribution d'énergie cinétique, en comparaison avec des études similaires sur la molécule isolée. Nous utilisons une nouvelle technique d'imagerie de photofragment pour mesurer simultanément la distribution angulaire et celle des vitesses. Il apparaît que la distribution d'énergie cinétique de l'iode atomique issu de la photodissociation de l'agrégat est notablement plus large et d'énergie plus basse que celle observée lors de la photodissociation du monomère. De plus la distribution angulaire est essentiellement isotrope dans le cas de l'agrégat alors qu'elle est fortement anisotrope dans le cas du monomère

keywords: clusters, photodissociation, kinetic energy, picosecond

Introduction

Free radicals are typically very reactive species and are often associated with exoergic chemistry.[1] Although they often require large energies of initiation, once formed, radicals are capable of sustaining a sequence of reactions involving breaking of strong bonds. Combustion and propulsion chemistry involves radical reactions initiated thermally at high temperature (i.e. H and O from H_2 and O_2).[2] Atmospheric chemistry, particularly ozone depleting cycles, is initiated by radicals generated photolytically (i.e. Cl from Cl_2 or HCl).[3]

Our clusters work seeks to better understand the connection between gas-phase and condensed-phase chemistry. This is a timely subject for radical chemistry. For example, the relationship between free radical chemistry in the gas phase and the condensed phase has attracted intense interest lately due to the discovery that polar stratospheric ozone depletion is aggravated by heterogeneous chemistry occurring on water and nitric acid trihydrate particles.[5] One can find many examples in nature of chemistry occuring at gas-liquid interfaces. Studies of analogous chemistry in clusters could very well provide crucial understanding of the correspondence between gas-phase and condensed-phase chemical properties.

In this paper, we focus on the photodissociation of CH_3I to CH_3 + I in the gas-phase[5–14] and in clusters.[15–19] The radicals initiated in the clusters lead to complex sequences of reactions that occur on the picosecond. Some issues that we address are: *i*- what are the products, *ii*- which products escape from the cluster (microscopic desorption), *iii*- what are the kinetic energies and angular distributions of escaping fragments such as I, and *iv*- how can collisional relaxation in clusters be measured? In this paper we introduce a new method for recording photofragment images of angle-velocity distributions and compare the results for the photofragment I atom dissociated from isolated CH_3I molecule versus from $(CH_3I)_n$ clusters. Finally, we describe a time-resolved photofragment imaging experiment that could yield valuable information on collisional relaxation in clusters.

Background

The following gas-phase photodissociation is a well studied reaction.[5–14]

$$CH_3I + h\nu \longrightarrow CH_3 + I\ (^2P_{3/2}, ^2P_{1/2}) \qquad (1)$$

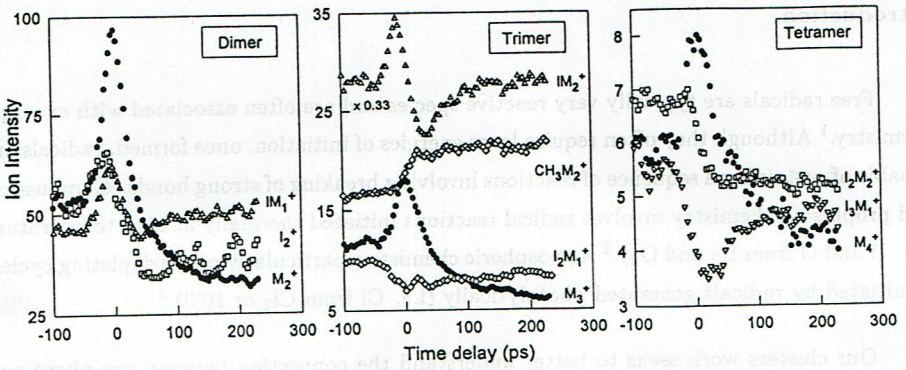

Figure 2. Picosecond measurements for photodissociation of M_n clusters (M = CH_3I). All traces are plotted on the same relative intensity scale. Note the offset in the ordinate. The time-dependence for loss of one CH_3 (IM_{n-1}, not shown for $n = 4$) is similar to the responses for $n = 2, 3$. Excitation was by 266-nm pump and 532-nm probe.

molecular chemistry. In an earlier picosecond pump-probe excitation/ionization experiment we observed rapid and extensive CH_3 radical initiated chemistry.[15,16] The experimental techniques are described in recent review articles.[20] Examples of picosecond pump-probe traces are given in Fig. 2 for the major products, which correspond to multiple loss of CH_3 radicals and single loss of I atom (which is the only I atom loss channel observed under our conditions). The time-dependences are complicated and vary for different species. These results suggest that extensive chemistry involving sequential reactions occurs over very short time scales. The parent cluster M_n (M = CH_3I) transient response is essentially symmetric and has a pulse convolved response time (FWHM) that matches the 40-ps cross-correlation time of the two pulses. The instrument-limited estimate of the reaction time is therefore < 10 ps. Production of IM_{n-1} and I_2M_{n-2} also occurs within the instrument response time. The IM^+_{n-1} signal exhibits a complicated dependence during the λ_1–λ_2 overlap period possibly indicating that this signal involves a reaction intermediate (cf. Sec. 4). The $I_2M^+_{n-2}$ signals for $n = 2 - 4$ in Fig. 2 display a sharp reduction at $t = 0$ to a constant level that persists to long delay times. The latter behavior suggests that dissociation takes place in the long-lived ion, presumably due to the I_2 (or I_2^+) component. However the sharp threshold indicates that the ion, and therefore the neutral product, is formed within the instrument resolution of 10 ps.[15]

The qualitative features in Fig. 2 indicate that the chemistry does not vary much with cluster size. We caution that size specificity is compromised because of evaporation of the ionized clusters, such that signal for smaller clusters can have contributions from larger clusters. We minimize this interference by adjusting expansion conditions so that the cluster

size distribution decreases with increasing n.

The fast-decay component for the parent $(CH_3I)_n$ cluster signals in Fig. 2 are followed by a slower 60-80 ps decay to a signal level below the 266-nm ionization baseline at negative delay time. A corresponding rise in the IM^+_{n-1} signal level also seems to occur. A possible explanation is that these responses reflect a 532-nm ion-photodissociation mechanism. The parent cluster ions M^+_n are formed with substantial excess energy by 3-photon ionization at 266 nm. It is possible that the cluster ions must await vibrational relaxation or nonradiative decay to an absorbing state. Nonradiative decay from the $\widetilde{A}$ to the $\widetilde{X}$ state of CH_3I^+ is estimated to be on the order of 100 ps,[21] which is consistent with the rate observed here. The possibility that the slow components are a neutral reaction channel, however, cannot be ruled out. These features need to be studied further.

Caging of I_2 and desorption of ethane

In our earlier time-resolved study of radical chemistry in $(CH_3I)_n$ clusters, we obtained evidence of a combustion or thermal runaway reaction mechanism.[15] The chemistry is assumed to be driven by the exothermicity of the reaction

$$CH_3I + CH_3I \longrightarrow C_2H_6 + I_2 \qquad \Delta H = -0.52 \text{ eV} \qquad (3)$$

A bottle of CH_3I clearly does not combust so one can safely conclude that the activation energy for the above reaction is very high. However, the reaction can be started by a radical mechanism that provides enough heat to sustain thermal chemistry. The cluster photoreactions were initiated by exciting into the dissociative $\widetilde{A}$ state of CH_3I. Gas-phase photodissociation to $CH_3 + I$ occurs in well under a picosecond with energy going almost entirely into translation.[11]

The 266-nm picosecond mass spectra in Fig. 3 show that the photoexcited clusters can lose a large number of CH_3 groups. Also evident in Fig. 3 is an alternation of peak intensities that are separated by two CH_3 mass units. Time-resolved measurements indicate that the multiple CH_3 loss channel is rapid. In Fig. 2c, the signal for I_3M_1, corresponding to loss of three CH_3 radicals (i.e., I_3M_{n-3} for $n = 4$), undergoes a rapid depletion at $t = 0$ within the instrument response time and then recovers for $t > 0$. Because the signal recovers, it is unlikely that the dissociation occurs in the long-lived ion, but rather in the short-lived

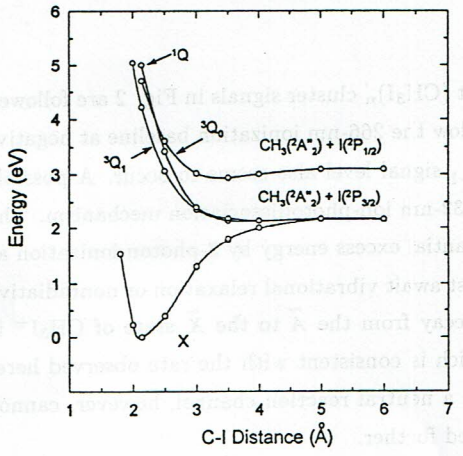

Figure 1. Potential energy curves for the ground electronic state X and the optically active dissociative A states. Symbols are calculated values from Tadjeddine *et al.* (Ref. 13).

Potential energy curves are presented in Fig. 1 based on calculated points by Tadjeddine *et al.*[13] The first excited electronic state (composed of several spin-orbit split subcomponents) is dissociative due to excitation of a $5pn \rightarrow \sigma^*$ electron. There are two dissociative channels corresponding to the ground and excited spin orbit states, $^2P_{3/2}$ and $^2P_{1/2}$ respectively, of I atom. The so called dissociative $\widetilde{A}$ states have a broad absorption spectrum peaking at about 260 nm.[10] At this wavelength, the dissociation lifetime is less than 100 fs, the photofragment angular distribution is highly anisotropic because dissociation is much faster than rotation, and nearly 80% of the available dissociation energy exits as fragment translational energy.[5–11]

Rates of methyl radical reactions in $(CH_3I)_n$ clusters

Because of the large mismatch in mass of the two fragments in CH_3I photodissociation, CH_3 carries away nearly all the available translational energy. Based on a photon energy of 4.66 eV, a C-I bond energy of 2.3 eV, and the relationship of fragment translational energy ϵ_i to total center-of-mass (c.m.) translational energy

$$\epsilon_i = \frac{m - m_i}{m}\epsilon_{cm} \tag{2}$$

where m_i is a fragment mass and m is molecular mass, one obtains values of ϵ_{CH_3} and ϵ_I of about 1.5 and 0.15 eV, respectively (for ground spin orbit state $^2P_{3/2}$ I atom).

Photodissociation in clusters can lead to caging of photofragments followed by inter-

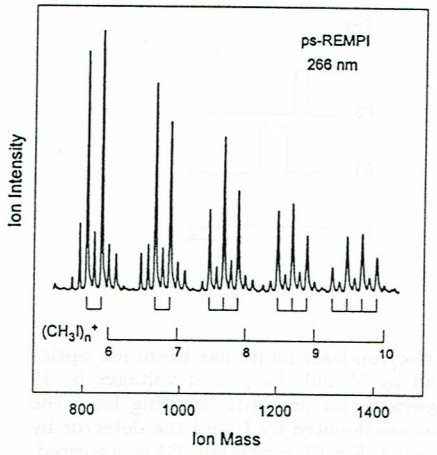

Figure 3. ps-resonance ionization mass spectra showing reactions in $(CH_3I)_n$ clusters. The major tic marks denote incremental cluster sizes and the minor tics denote sequential loss of ethane.

neutral. The $I_3M_1^+$ response is strong evidence for a neutral reaction mechanism.

The picosecond results summarized here and detailed elsewhere are consistent with a reaction mechanism based on the chemistry of CH_3 radical. 266-nm excitation exceeds the C-I bond energy by about 2.3 eV. The excess energy is released mainly as kinetic energy in the CH_3 radical,[5] which can then react as follows

$$[CH_3 + (CH_3I)_{n-1}] \longrightarrow C_2H_6 + I(CH_3I)_{n-2} \qquad \Delta H = -1.37\ eV \qquad (4)$$

where we assume that the photodissociated I atom is lost (recombination of I atoms would contribute an additional exothermicity of $\Delta H = -1.58$ eV). An alternative pathway to production of ethane involves the absorption of two photons by $(CH_3I)_n$ to produce two CH_3 radicals that recombine to release 3.81 eV of heat. In either case, the heat of reaction, augmented by the initial radical kinetic energy and recombination of I atoms, can drive additional chemistry involving exothermic formation of ethane. The hot cluster product above, for example, could undergo the thermal rearrangement

$$I(CH_3I)_{n-2} \longrightarrow C_2H_6 + I_3(CH_3I)_{n-4} \qquad \Delta H = -0.52\ eV \qquad (5)$$

The additional heat fuels further loss of ethane. Subsequent photodissociation could also enhance the rate of C-I bond breaking and exothermic production of C_2H_6.

It is interesting to note that despite extensive demethylation, there is very little loss of

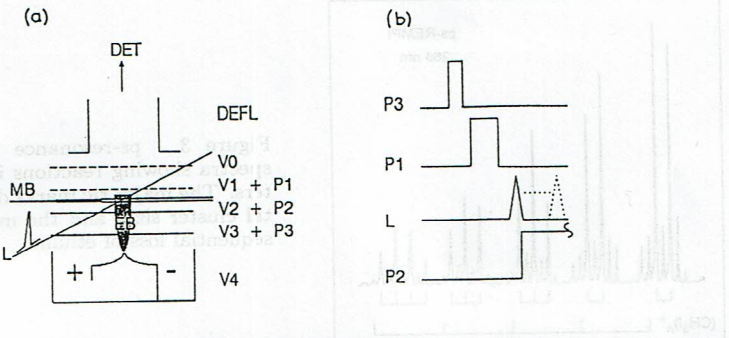

Figure 4. (a) Configuration of the crossed electron-laser-molecular beam ion optics assembly. The grid voltages are designated by V and the pulsed voltages by P. Deflector plates (DEFL) are used to compensate for ion drift resulting from the molecular beam (MB) velocity. Laser pulses are denoted by L and the detector by DET. (b) Low mass filter (LMF) pulse sequence. For EI excitation, P3 is activated. For MPI, a laser pulse is fired instead of P3.

iodine atoms from the clusters. Apparently the heavy mass is efficiently caged. Part of the reason for this may be due to the kinematics of a heavy-light dissociation where the light fragment carries off a substantial fraction of the dissociative translational energy according to Eq. (2). A particularly interesting reaction is the product of the major product I_2. Vaida, *et al.* suggested that I_2 is produced in $(CH_3I)_n$ clusters on the basis of the detection of I_2^+ following nanosecond resonance ionization through the valence $\tilde{A}$ state.[17] These results, however, did not distinguish between I_2^+ formed by ionization of neutral product I_2 or by dissociation of cluster ions. This competition is a concern in cluster research because the weak van der Waals (vdW) bonds usually mean that both neutral and ionic dissociation will occur. Picosecond pump-probe measurements help to sort out these competitive processes because they usually occur over different timescales.[16] However, we also take the independent approach of measuring directly the ion dissociation mechanisms by electron-impact (EI) ionization and by mass-selective ion photodissociation. The ion photodissociation experiments make use of a crossed electron-laser-molecular beam configuration as shown in Fig. 4. The molecular clusters are first ionized by EI excitation, then mass filtered, and finally resonantly photodissociated using nanosecond laser pulses.[22,23]

The methodology behind using both resonance ionization and direct ionization to identify neutral cluster reactions is illustrated in Fig. 5 for $(CH_3I)_n$ clusters. EI ionization is used to ionize the clusters directly in order to ascertain fragment ions that occur exclusively by ion dissociation mechanisms. The electron beam flux is sufficiently low that all excitation events occur by a single electron. The EI mass spectrum in Fig. 5a shows that dissociation following cluster ionization consists only of C–I bond breaking or van der Waals (vdW) evaporation. The operation of the TOF low mass rejection filter is illustrated in Fig. 5b

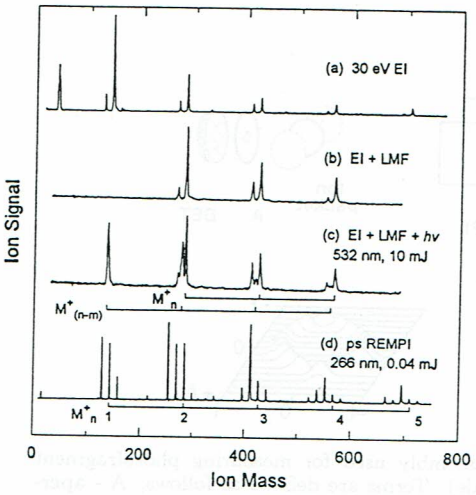

Figure 5. $(CH_3I)_n$ cluster ionization mass spectra (M = CH_3I). (a) Direct ionization by EI excitation at 30 eV. (b) EI ionization and low mass filter (LMF). (c) Same, but with resonant photodissociation of cluster ions. (d) Picosecond $\tilde{A}$ state REMPI.

where all masses less than the dimer mass are rejected from the excitation volume. (The details of this device are described elsewhere.)[7] In Fig. 5c, the remaining ions are excited by a laser pulse that is resonant with a predissociative absorption in CH_3I. This excitation, which is known to cleave the C–I bond in monomer CH_3I^+ results only in vdW dissociation in the cluster ions. It is not surprising that the weakest bond breaks. (In Sec. 5.2 we present an example of a cluster ion dissociation in which a strong bond breaks preferentially to a weak bond.) Finally, Fig. 5d contains the picosecond mass spectrum of $(CH_3I)_n$ resulting from excitation of the dissociative $\tilde{A}$ state. A distinctly different spectrum is observed from the ion fragmentation spectra in Figs 5a-c. As a result of the overall procedure encompassed by Fig. 5, the additional signals in Fig. 5d can be assigned to ionization of *neutral* reaction products.

Recent work by Ziegler, *et al.*[18] and Fan and Donaldson, *et al.*[19] show that on the nanosecond timescale thermally hot I_2 is observed free of the clusters (although the excitation energy and, therefore, the I_2 energy content differ in these two studies). It will be interesting in a future time-resolved experiment to measure the rate of production of I_2 in the cluster and the subsequent rate of evaporation or separation from the cluster. Perhaps I_2 in different vibrational levels will show different time dependences reflecting some diversity of the local environment in clusters.

Kinetic energy release and angular distribution of I fragment

Our results indicate that extensive chemistry occurs in a time short compared to

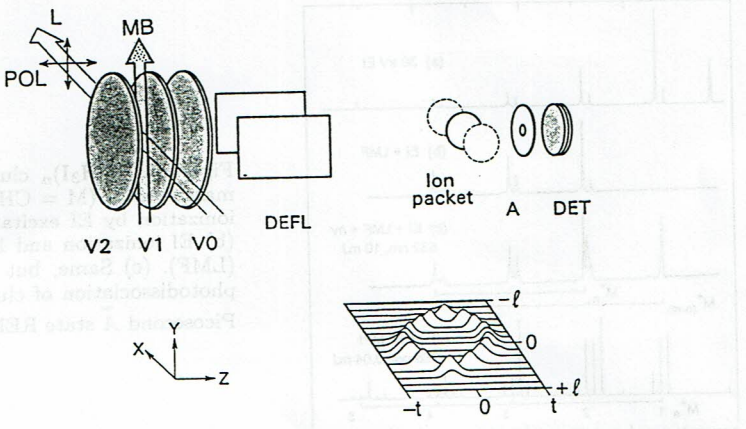

Figure 6. Time-of-flight ion optics assembly used for measuring photofragment angle-velocity distributions (not to scale). Terms are defined as follows: A - aperture, DEFL - ion deflector plates, DET - detector; L - laser, MB - molecular beam; POL - laser polarization axis; V0, V1, V2 - ion acceleration grids. Deflector plates for y-axis are not shown. A simulated spectrum is illustrated for the xz plane.

evaporation. However, over the mass spectrometer response time evaporation certainly occurs. For example, the mass spectra in Fig. 3 indicate that extensive methyl loss occurs by way of ethane escape from the cluster. As noted above, iodine is efficiently caged such that the only sigificant iodine loss channel is limited to a single atom.

It is interesting to compare the properties of I atom loss from $(CH_3I)_n$ clusters versus that from bare CH_3I. The latter reaction has been extensively studied by $\tilde{A}$ state excitation and has the properties of a prompt dissociation (<100 fs), a large anisotropy in the product angular dependence relative to the laser polarization axis, and a large fraction of excess energy released as kinetic energy.[5–11]

We begin by describing a new molecular beam technique for directly recording two-dimensional images of the three-dimensional product angle-velocity distribution. A more complete description is given elsewhere.[14] The method is similar in spirit to that of Houston and Chandler[24] except that our images are recorded in the form of slices rather than projections of the 3D angle-velocity distributions. As illustrated in Fig. 6, molecules are photodissociated and products subsequently ionized by laser excitation. The expanding ion packet (shown as a sphere in this example) represents the three-dimensional angle-velocity distribution. A series of time-of-flight spectra are collected using a rastering procedure that sweeps the ionized photoproduct packet across a detector aperature by electric field deflection.

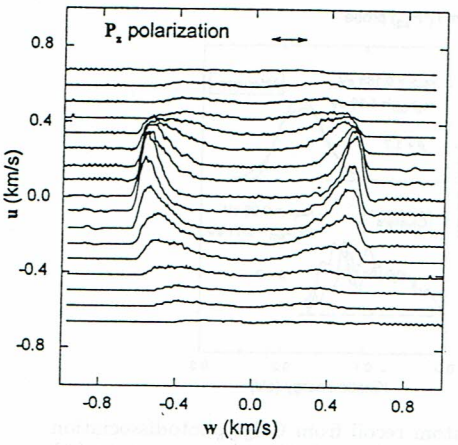

Figure 7. Measurements of the 2D angle-velocity image of the I($^2P_{3/2}$) atom fragment from photodissociation of CH_3I at 266 nm by parallel excitation. The w and u axes are the center-of-mass velocity components parallel and perpendicular to the laser polarization axis, respectively. The intensity axis is out-of-plane.

In the present experiments, photodissociation is initiated at 266 nm and I atom is probed by 2+1 resonance enhanced multiphoton ionization (REMPI) at 304.7 nm ($^2P_{3/2}$ spin orbit state) or 304.0 nm ($^2P_{1/2}$ state).[25] These experiments are presently not time-rseolved. However, a time-resolved photofragment imaging experiment is discussed shortly. The photofragment image for I atom from bare CH_3I photodissociation is shown in Fig. 7. A strong forward-backward peaked angular distribution is observed. The product flux is aligned with the laser polarization axis indicating that photodissociation occurs predominately from a parallel transition. Similar spectra were recorded for the I($^2P_{1/2}$) state, for 304 nm photolysis, and for perpendicular polarization.[14] Product velocities are measured from the time-of-flight (TOF) distributions of the ionized product I atoms. The most probable recoil angles for a parallel transition, having the laser polarization aligned along the ion drift-tube axis, are toward and away from the detector. The ionized products initially going away from the detector are slowed and turned around by the extraction field and arrive at the detector delayed in time with respect to the products initially going toward the detector. Under space focussing conditions, velocity is related directly to time delay by the expression

$$v = q\mathcal{E}\Delta t/m \tag{6}$$

where $\mathcal{E}$ is the extraction field and Δt is the displacement in time from the center position.

We recorded TOF spectra for the I atom photofragment for excitation at different times within the gas pulse. The times in Figs. 8A-C refer to the delay between the laser pulse and the leading edge of a nominally 400-μs gas pulse. Monomers dominate early

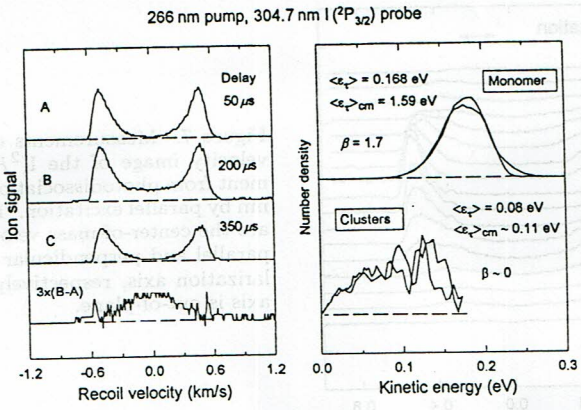

Figure 8. TOF mass spectra showing I atom recoil from CH_3I photodissociation. The abscissa has been converted to velocity using Eq. (6). The times in spectra (A)-(C) refer to the delay between the laser pulse and the leading edge of a nominally 400-μs gas pulse. (Right panel) Kinetic energy distribution for CH_3I and $(CH_3I)_n$. The mean center-of-mass kinetic energy $\langle \epsilon_t \rangle_{cm}$ for clusters assumes an average size of $n = 3$. β is the anisotropy factor. The results for both lobes of the TOF recoil velocity spectra are superimposed on the kinetic energy plots.

and late in the gas pulse because of the lower density of molecules, the warmer expansion temperature, and for the early time leading edge because the heavier clusters lag behind the monomers in the molecular beam due to slip. It is evident in Fig. 8A from the absence of low velocity component I atoms that dissociation occurs almost exclusively from monomer. Excitation in the middle of the gas pulse, where the formation of clusters is greatest, leads to dissociation of low-energy I atoms. We have extracted an I atom velocity distribution for cluster photodissociation by subtracting spectrum A from B in Fig. 8. These are preliminary cluster results since they were recorded to establish conditions for minimizing cluster formation for monomer photodissociation measurements such as that in Fig. 7. The series of TOF traces in Fig. 8 were recorded with a moderately large detector field-of-view (i.e., controlled by aperture diameter and ion drift velocity), which diminishes the resolution orthogonal to the drift tube. This is evident by noting that the forward-backward peak in the centerline trace in Fig. 7 is much sharper than it is in Fig. 8A. Nonetheless, the results in Fig. 8 are useful for demonstrating how kinetic energy distributions can be measured for cluster photodissociations.

The TOF spectra recorded here represent measurements of the distribution of the velocity component along the drift tube z-axis, $P(v_z)$. A single TOF trace is therefore a 1D measurement. A 1D projection is recorded if the detector field-of-view is sufficiently large to collect all ions irrespective of their velocity orthogonal to the drift tube axis. A 1D slice is recorded if the detector aperture is sufficiently small so that only a narrow range

of orthogonal velocity components are collected. The image in Fig. 7 is comprised of a series of 1D slices. The quantity of interest is the number density or fraction of product $f(v)$ with velocity between v and $v + dv$. This function, sometimes referred to as the speed distribution, represents the radial dependence of $P(v)$.[26] For a 1D projection of an isotropic distribution, $f(v)$ is given by

$$f(v)dv = P(v)4\pi v^2 dv \tag{7}$$

Determination of $f(v)$ from an anisotropic distribution is more complicated and requires a fitting routine. The problem simplifies considerably by evaluating a 1D slice rather than a projection of the total angular distribution. In Fig. 7 this corresponds to evaluating $f(v)$ from the centerline trace $I(v)$ rather than from the sum of traces. The speed distribution is then obtained from the expression

$$f(v)dv = I(v)vdv \tag{8}$$

The low resolution 1D TOF trace for monomer fragments in Fig. 7A is not sufficiently resolved to qualify as a 1D slice $I(v)$. Instead, we apply Eq. (8) to higher resolution TOF spectra such as the one corresponding to the centerline trace in Fig. 7. Because cluster photodissociation leads to low energy ions, the $P(v)$ distribution for clusters is best described as a 1D projection and can be analyzed using Eq. (7). The kinetic energy distributions in Fig. 8 are obtained by plotting $f(v)$ vs $mv^2/2$ and mean kinetic energies $\langle \epsilon_t \rangle$ are obtained from the expression

$$\langle \epsilon_t \rangle = \frac{m}{2} \frac{\int v^2 f(v) dv}{\int f(v) dv} \tag{9}$$

The I atom kinetic energy distribution peaks at a much lower value for cluster than for monomer photodissociation. This difference is more pronounced when converted to a center-of-mass kinetic energy by Eq. (2). Because m depends on cluster size and we do not achieve size-specific excitation in this particular experiment, we must assume an average m for the cluster photodissociations results. From low-energy electron impact ionization mass spectra we estimate an average cluster size of $n = 3$. The values of $\langle \epsilon_t \rangle_{cm}$ reported in Fig. 8 are, therefore, based on monomer and trimer photodissociation. The anisotropy parameter β is obtained by fitting the angular dependence of the I atom signal to the expression

$$P(\theta,\phi) = \frac{1}{4\pi}\left[1+\frac{\beta}{2}(3\cos^2\theta - 1)\right] \quad (10)$$

where θ is the angle between the laser polarization and drift-tube axis, and ϕ is the azimuthal angle about the drift-tube axis, which in this case is invariant to θ. The monomer dissociation is highly aligned along the laser polarization axis and has an anisotropy of $\beta = 1.7$ close to the maximum value of 2, which is consistent with previous investigations [63-65]. This is to be contrasted with the cluster dissociation, which is essentially isotropic $\beta \sim 0$. The low-energy isotropic distribution of I atom from clusters is indicative of a dissociation that is not impulsive. Apparently dissociated I atoms undergo collisions within the clusters that relax much of the initial kinetic energy and delay their escape sufficiently long for rotations to occur. In a sense, I atoms are thermalized in the cluster, some of them recombining to form I_2 and some escaping. Because these experiments probe I atom and, therefore, do not distinguish specific cluster sizes, it is not yet possible to determine the cage versus escape probability.

Time-resolved photofragment imaging

We close by proposing a new experiment that measures collisional relaxation in clusters. One sees in Fig. 8 the very different angular and kinetic energy distributions of I atom photodissociated from a bare molecule versus from a cluster. An important question is what would be observed if we detected I atom photofragment that escaped from clusters at very early times. Presumably, the angle-velocity distribution would resemble that of bare molecule, because these early fragments either were pointed away from the cluster bulk or escaped with minimal collisional interaction. Also the fragment translational energy may be greater than for photodissociation of the bare molecule because the counter fragment is not a light CH_3 group but a heavy cluster group containing CH_3 [cf. Eq. (2)]. As one recorded time-resolved photofragment images as a function of pump-probe delay time, one might expect an angle-velocity distribution that evolved in time from anisotropic and high translational energy to isotropic and low translational energy. This evolution in time would be due to collisional relaxation of the I atom during the time it resided in the cluster. Consequently, the measured decrease in I atom kinetic energy with time is actually a measure of the rate of collisional relaxation of I atom translational energy in the cluster.

We leave aside for the moment the interesting issue of the rate of loss of anisotropy with time and speculate on the simpler dependence of fragment kinetic energy versus residence

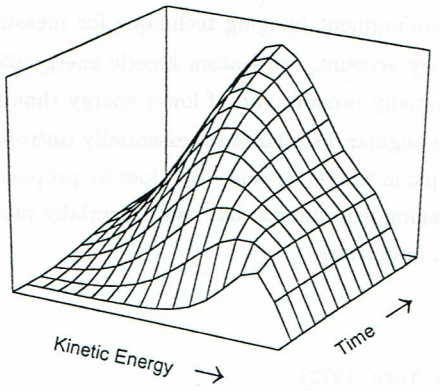

Figure 9. A schematic of the expected trend in fragment kinetic energy distribution from cluster photodissociation as a function of pump-probe delay time. The decrease in fragment kinetic energy with increasing time represents collisional relaxation of the fragment during its residence in the cluster.

time in the clusters. Fig. 9 is a schematic of what one might expect to observe. At very early times, the fragment should resemble that of a prompt photodissociation and have a kinetic energy distribution strongly peaked at high energy. By increasing the pump-probe delay time, fragments of increasingly longer residence time in the cluster appear in the measurement. These will have kinetic energy distributions that become broader and shift to lower energy as seen in Fig. 9. This evolution is more apparent by subtracting the measured distributions for different time delays, thereby plotting the differential changes for discrete time intervals rather than the cumulative changes. The measured decrease of fragment kinetic energy with delay time is believed to directly measure the collisional relaxation rate in clusters. Such a measurement would provide another valuable set of data to compare to bulk-phase measurements and potential lead to a better understanding of solvation effects on a single molecule level.

Summary and Conclusions

We have presented a study of the photodissociation of CH_3I to $CH_3 + I$ in an isolated molecule and in clusters. We began by reviewing our picosecond pump-probe studies of the photodissociation in clusters. This work revealed very fast sequential radical chemistry. An important recurring reaction is $CH_3 + CH_3I \rightarrow C_2H_6 + I$. Extensive methyl loss through this ethane formation mechanism occurs that ultimately evaporates from the clusters. On the other hand, iodine escape from the cluster was much less common. A single I atom loss was the predominate reaction.

The new results presented here are measurements of the I atom anisotropy and kinetic energy distribution from cluster photodissociation and the comparison to similar measure-

ments in bare CH_3I. We describe a new photofragment imaging technique for measuring angle-velocity distributions. In this preliminary account, the I atom kinetic energy distribution for cluster photodissociation is substantially broader and of lower energy than that observed for monomer photodissociation. The angular distribution is essentially isotropic in the former case as opposed to highly anisotropic in the latter case. We close by proposing a time-resolved pump-probe photofragment imaging experiment that can potentially provide a direct measurement of collisional relaxation in clusters.

References

1. J. K. Kochi, *Free Radicals,* (Wiley, New York, 1973).

2. W. C. Gardiner, Jr., editor *Combustion Chemistry,* (Springer-Verlag, New York, 1984).

3. R. P. Wayne, *Chemistry of Atmospheres,* 2nd Ed. (Clarendon Press, Oxford, 1991); B. J. Finlayson-Pitts and J. N. Pitts, Jr. *Atmospheric Chemistry,* (Wiley, New York, 1986).

4. J. G. Anderson, D. W. Toohey, and W. H. Brune, *Science* **251,** 39 (1991).

5. R. K. Sparks, K. Shobatake, L. R. Carlson, and Y. T. Lee, *J. Chem. Phys.* **75,** 3838 (1981).

6. G. N. A. van Veen, T. Baller, A. E. de Vries, and N. J. A. van Veen, *Chem. Phys.* **87,** 405 (1984). M. D. Barry and P. A. Gorry, *Mol. Phys.* **52,** 461 (1984).

7. R. Ogorzalek Loo, H.-P. Haerri, G. E. Hall, and P. L. Houston, *J. Chem. Phys.* **90,** 4222 (1989); R. Ogorzalek Loo, G. E. Hall, H.-P. Haerri, and P. L. Houston, *J. Phys. Chem.* **92,** 5 (1988).

8. S. M. Penn, C. C. Hayden, K. J. Carlson Muyskens, and F. F. Crim, *J. Chem. Phys.* **89,** 2909 (1988). J. F. Black and I. Powis, *Chem. Phys.* **125,** 375 (1988).

9. D. W. Chandler and P. L. Houston, *J. Chem. Phys.* **87,** 1445 (1987). D. W. Chandler, J. W. Thoman, Jr., M. H. M. Janssen, and D. H. Parker, *Chem. Phys. Lett.* **156,** 151 (1989).

10. A. Gedanken and M. D. Rowe, *Chem. Phys. Lett.* **34,** 39 (1975); A. Gedanken, *Chem. Phys. Lett.* **137,** 462 (1987).

11. J. L. Knee, L. R. Khundkar, and A. H. Zewail, *J. Chem. Phys.* **83,** 1996 (1985).

12. R. S. Mulliken, *J. Chem. Phys.* **8,** 382 (1940); *ibid.* **3,** 513 (1935); M. Shapiro, *J. Phys. Chem.* **90,** 3644 (1986).

13. M. Tadjeddine, J. P. Flament, and C. Teichteil, *Chem. Phys.* **118,** 45 (1987); S. K.

Gray and M. S. Child, *Mol. Phys.* **51,** 189 (1984).

14. R. A. Hertz and J. A. Syage, *J. Chem. Phys.* **100,** 9265 (1994). R. A. Hertz and J. A. Syage, *Proc. SPIE-Int. Soc. Opt. Eng.* **2124,** 187 (1994).
15. J. A. Syage and J. Steadman, *Chem. Phys. Lett.* **166,** 159 (1990).
16. J. Steadman, E. W. Fournier, and J. A. Syage, *Appl. Opt.* **29,** 4962 (1990).
17. S. P. Sapers, V. Vaida, and R. Naaman, *J. Chem. Phys.* **88,** 3638 (1988).
18. P. G. Wang, Y. P. Zhang, C. J. Ruggles, and L. D. Ziegler, *J. Chem. Phys. 92,* 2806 (1990).
19. Y. B. Fan and D. J. Donaldson, *J. Phys. Chem.* **96,** 19 (1992).
20. J. A. Syage, in *Ultrafast Spectroscopy in Chemical Systems,* edited by J. D. Simon (Kluwer Academic Publishers, New York, 1993), p. 289.; J. A. Syage, *Femtosecond Chemistry,* edited by J. Manz and L. Wöste (VCH Publishers, New York, 1994).
21. S. P. Goss, J. D. Morrison, and D. L. Smith, *J. Chem. Phys.* **1981,** *75,* 757.
22. J. A. Syage, *J. Chem. Phys.* **92,** 1804 (1990).
23. J. A. Syage and J. Steadman, *Rev. Sci. Instrum.* **61,** 1204 (1990).
24. D. W. Chandler and P. L. Houston, *J. Chem. Phys.* **87,** 1445 (1987). D. W. Chandler, J. W. Thoman, Jr., M. H. M. Janssen, and D. H. Parker, *Chem. Phys. Lett.* **156,** 151 (1989).
25. Y. Jiang, M. R. Giorgi-Arnazzi, and R. B. Bernstein, *Chem. Phys.* **106,** 171 (1986).
26. W. J. Moore, *Physical Chemistry,* 4th ed., (Prentice-Hall, Englewood Cliffs, 1972), p. 130 ff.